Electron-phonon interaction in hole-doped MgB_2C_2

E. Spanò and M. Bernasconi
Consorzio Corimav, Dipartimento di Scienza dei Materiali, Università di Milano-Bicocca, Via Cozzi 53, I-20125 Milano, Italy

E. Kopnin
Pirelli Labs, Viale Sarca 336, I-20126 Milano, Italy
(Received 24 February 2005; published 19 July 2005)

Based on density functional perturbation theory, we predict that hole-doped MgB_2C_2, which is isoelectronic and structurally similar to MgB_2, has a strong electron-phonon coupling constant. By substituting Mg atoms with alkali metals (Li,Na), pristine insulating MgB_2 turns metallic with holes in the σ bands at the Fermi level. Calculation of the formation enthalphies show that hole-doped $Li_xMg_{(1-x)}B_2C_2$ or $Na_xMg_{(1-x)}B_2C_2$ for $x=0.125$–0.25 might be synthesized experimentally under conditions of Mg deficiencies. We find that the contribution of the σ bands to the electron-phonon coupling constant of $Li_{0.125}Mg_{0.875}B_2C_2$ is $\Lambda_{\sigma\sigma}=0.91$, due to the modulation of the σ bands produced by stretching modes of the borocarbide hexagonal planes. Based on *ab initio* phonons and electron-phonon coupling constants, we estimate from the McMillan formula a value for superconductive T_c of 67 K (for $\mu^*=0.1$), higher than that of MgB_2 mainly because of larger phonon frequencies ($\omega_{ln}=777$ cm^{-1}).

DOI: 10.1103/PhysRevB.72.014530 PACS number(s): 74.25.Kc, 74.25.Jb, 74.70.Ad

I. INTRODUCTION

The discovery of superconductivity[1] in MgB_2 at 36 K has led to a resurgence of interest in superconductivity of low-Z materials, metallic or made metallic by doping. On the basis of *ab initio* calculations, Rosner *et al.*[2] have recently suggested that hole doping of insulating LiBC, isovalent with and structurally similar to MgB_2, generates a Fermi surface with a strong electron-phonon interaction. This is due to the modulation of σ bands at the Fermi surface by a stretching mode of the B-C bond which is the same feature that leads to high-T superconductivity in MgB_2.[3,4] For $Li_{0.5}BC$, the electron-phonon coupling constant λ has been estimated theoretically to be 1.8 times larger than in MgB_2 which would lead to a rather high T_c (100 K).[2,5] Hole doping has been proposed theoretically to lead to high-T_c superconductivity in BC_3 as well.[6] Several attempts have been made experimentally to hole-dope LiBC with Li deficiencies, but no convincing evidence for superconductivity has be established so far.[7–10] A biphasic material made by LiBC and amorphous graphiticlike carbon has been proposed to be formed upon Li deintercalation.[9] These difficulties in hole doping might be less severe in MgB_2C_2, another compound isoelectronic with and structurally similar to MgB_2 and LiBC.[11] MgB_2C_2 is insulating, but it has been predicted to turn metallic by hole doping via partial substitution of divalent Mg with alkali metals.[12] Band structure calculations of the compounds $Mg_{(1-x)}A_xB_2C_2$ (with $x=0.5$, A=Li,Na,K) show that the Fermi surface is similar to that of MgB_2, involving σ bands, nearly flat along the direction perpendicular to the BC hexagonal layers.[12]

In the present work, we have investigated further the properties of hole-doped MgB_2C_2. Based on *ab initio* calculations we have computed the formation energy and equilibrium structure of the compounds $Mg_{(1-x)}Li_xB_2C_2$, $Mg_{(1-x)}Na_xB_2C_2$, and $Mg_{(1-x)}B_2C_2$ to assess their stability at different doping levels with respect to phase separation in other products. The vibrational properties and electron-phonon coupling constant λ have been computed within density functional perturbation theory (DFPT).[13] For $Mg_{0.875}Li_{0.125}B_2C_2$ the estimated electron-phonon coupling constant is close to that reported for MgB_2.[4] These results suggests that hole-doped MgB_2C_2 might be another boron-based material with interesting superconductive properties as speculated in previous works.[12]

II. COMPUTATIONAL DETAILS

Calculations are performed within the framework of density functional theory with a gradient-corrected exchange and correlation energy functional,[14] as implemented in the codes PWSCF and PHONONS.[15] Norm-conserving pseudopotentials[16] and plane-wave expansion of Kohn-Sham (KS) orbitals up to a kinetic cutoff of 40 Ry have been used. Nonlinear core corrections are included in the pseudopotentials of magnesium and alkali metals.[17] Brillouin zone (BZ) integration has been performed over Monkhorst-Pack (MP) meshes.[18] Hermite-Gaussian smearing of order 1 with a linewidth of 0.01 Ry has been used for metallic compounds.[20] Equilibrium geometries have been obtained by optimizing the internal and lattice structural parameters at several volumes and fitting the energy versus volume data with a Murnaghan function.[19] Residual anisotropy in the stress tensor at the optimized lattice parameters at each volume is below 1.0 kbar. To assess the stability of hole-doped MgB_2C_2 with respect to formation of other compounds we have also computed the formation energy of LiBC, B_4C, Na_2B_{29}, Na_3B_{20}, α-B, diamond, and metallic Na and Li.[22] Phonons at the Γ point have been computed within DFPT.[13] Details on

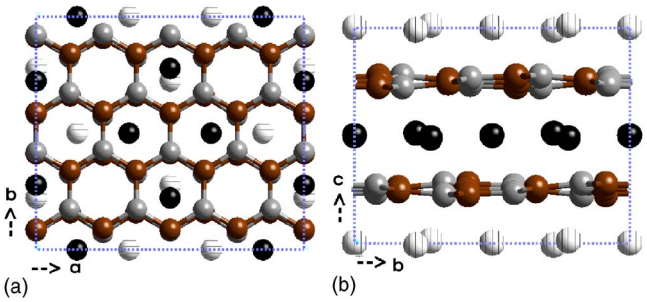

FIG. 1. (Color online) Crystal structure of MgB_2C_2. (a) (001) view of the *ab* plane. (b) Puckering of the [BC] layers in a (100) projection on the *cb* plane. Boron, carbon, and magnesium are represented by gray, dark gray, and black (or shaded white) spheres, respectively. The Mg is represented with different color at different heights.

the calculation of the electron-phonon coupling constant are given in Sec. III B.

III. RESULTS

A. Structural and electronic properties

MgB_2C_2 crystallizes in an orthorhombic structure with space group $Cmca(D_{2h}^{18})$. The unit cell contains eight formula units (40 atoms) and eight atoms independent by symmetry. The structure of MgB_2C_2 is shown in Fig. 1. The experimental and theoretical lattice structural parameters are compared in Tables I and II. The borocarbide hexagonal layer is not flat, but slightly puckered with a maximum deviation of 0.2 Å from the optimized plane. The Mg cations are coordinated by six boron and carbon atoms forming a slightly distorted hexagonal prism. The cations are not distributed uniformly between the borocarbide layers, but show local clustering of four Mg atoms which are surrounded by nonoccupied hexagonal prismatic voids. The Mg clusters in adjacent layers are shifted as shown in Fig. 1(b).

The theoretical equilibrium geometry reported in Tables I and II is obtained by fully optimizing all the structural parameters and fitting the energy-versus-volume points with a Murnaghan function.[19] The resulting theoretical bulk modulus and derivative of the bulk modulus with respect to pressure at equilibrium are $B=134$ GPa and $B'=3.287$. The agreement between theoretical and experimental structural parameters is very good (Tables I and II). The theoretical corrugation of the borocarbide planes (0.19 Å) is also very close to the experimental value (0.2 Å, Ref. 11).

TABLE I. Calculated equilibrium lattice parameters (Å) of pristine MgB_2C_2 and hole-doped compounds. Experimental data for MgB_2C_2 are from Ref. 11.

System	*a*	*b*	*c*
MgB_2C_2 expt.	10.92	9.46	7.46
MgB_2C_2	10.89	9.42	7.33
$Mg_{0.875}B_2C_2$	10.92	9.43	7.54
$Li_{0.125}Mg_{0.875}B_2C_2$	10.87	9.42	7.36
$Li_{0.25}Mg_{0.75}B_2C_2$	10.84	9.40	7.42
$Li_{0.5}Mg_{0.5}B_2C_2$	10.80	9.40	7.45
$Na_{0.25}Mg_{0.75}B_2C_2$	10.80	9.32	7.70

The electronic band structure of MgB_2C_2 is reported in Fig. 2(a) along the high-symmetry lines in the irreducible part of the Brillouin zone (IBZ, see Fig. 3). The system is insulating with an indirect band gap of 1.4 eV, in agreement with previous calculations.[12] The flat bands along the Γ-Z direction, perpendicular to the borocarbide hexagonal planes, are reminiscent of the band structure of MgB_2. As inferred from the analysis of the projection of KS orbitals on atomic pseudo-wave-functions, these flat bands are formed by bonding B-C σ orbitals, but as opposed to MgB_2, they are completely filled as occurs in LiBC.[2] By substituting divalent Mg with alkali metals, hole are introduced in the σ bands as shown in Figs. 2(b)–2(e) for the compounds $A_xMg_{(1-x)}B_2C_2$ (A=Li, Na). The compound $Li_{0.125}Mg_{0.875}B_2C_2$ is obtained by substituting with Li one Mg atom per cell at position 8*f*. The compound $Li_{0.25}Mg_{0.75}B_2C_2$($Na_{0.25}Mg_{0.75}B_2C_2$) is obtained by substituting with Li (Na) two Mg atoms per cell both at positions 8*f*. The distribution of alkali metals in a single plane in $Li_{0.125}Mg_{0.875}B_2C_2$ and $Li_{0.25}Mg_{0.75}B_2C_2$ is shown in Fig. 4. We have also considered a highly ordered compound $Li_{0.5}Mg_{0.5}B_2C_2$ in which metallic planes of Li alternate with metallic planes of Mg. As opposed to the calculations in Ref.

TABLE II. Calculated coordinates of the eight atoms independent by symmetry in MgB_2C_2 (in crystal units). The experimental data from Ref. 11 are given in parentheses. Theoretical average effective charges $Z^*=(1/3)\mathrm{Tr}\underline{\underline{Z}}^*$ (see Sec. III B) are also given (in a.u.).

	x	*y*	*z*	Z^*
Mg (8*d*)	0.15315 (0.1534)	0	0	1.980
Mg (8*f*)	0	0.2769 (0.2798)	−0.0110(−0.0113)	1.868
B1 (8*e*)	1/4	0.0934 (0.0946)	1/4	1.663
B2 (8*f*)	0	0.5879 (0.5886)	0.2741 (0.2760)	1.331
B3 (16*g*)	0.1275 (0.1278)	0.3404 (0.3415)	0.2433 (0.2438)	1.527
C1 (8*e*)	1/4	0.9263 (0.9271)	1/4	−2.493
C2 (8*f*)	0	−0.0797(−0.0792)	0.2342 (0.2314)	−2.471
C3 (16*g*)	0.1245 (0.1245)	0.1740 (0.1750)	0.2239 (0.2231)	−2.396

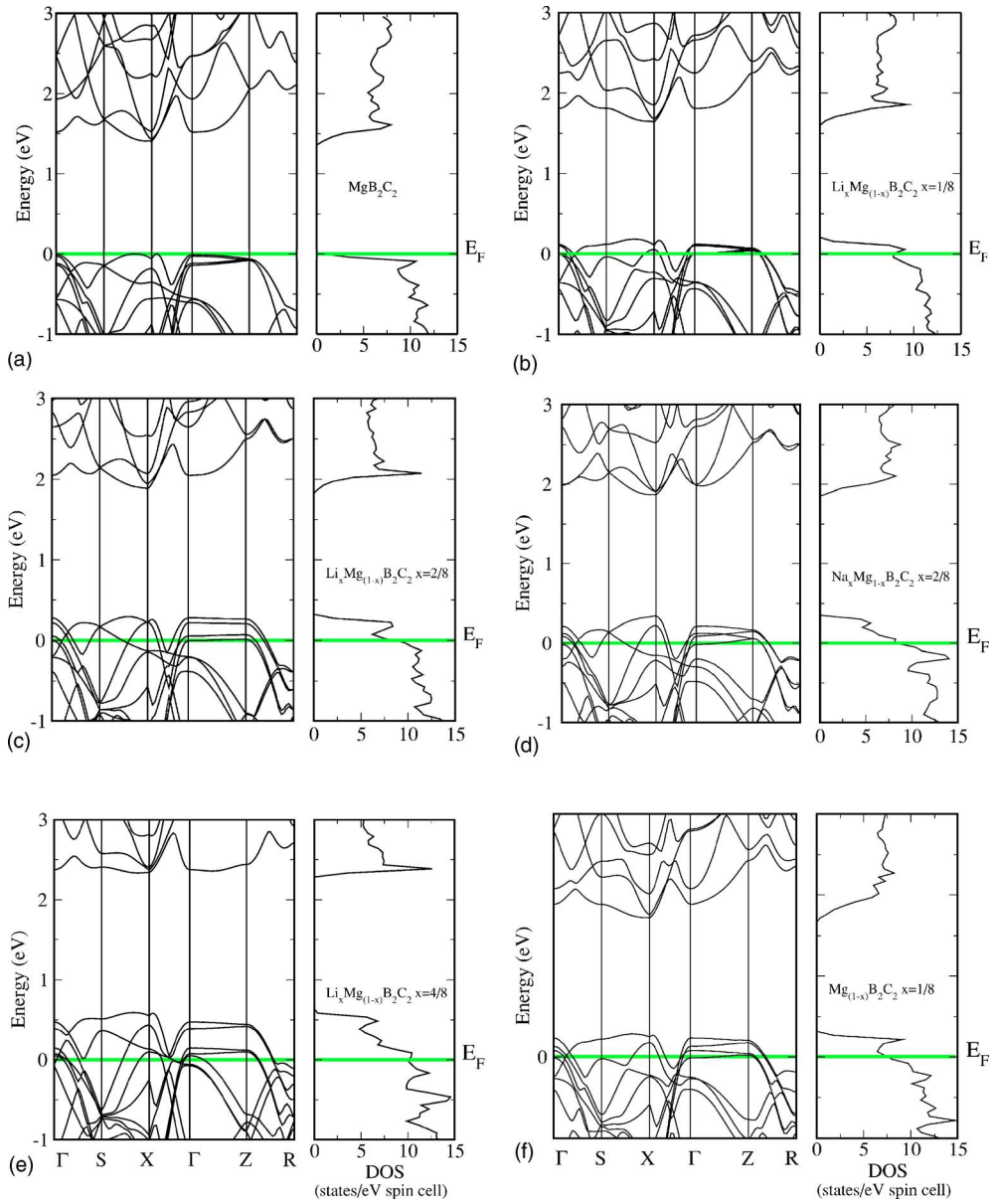

FIG. 2. (Color online) Electronic band structure and density of states of (a) MgB_2C_2, (b) $Li_{0.125}Mg_{0.875}B_2C_2$, (c) $Li_{0.25}Mg_{0.75}B_2C_2$, (d) $Na_{0.25}Mg_{0.75}B_2C_2$, (e) $Li_{0.5}Mg_{0.5}B_2C_2$, and (f) $Mg_{0.875}B_2C_2$. The zero of energy is the Fermi level. The density of states is computed by the tetrahedron method with 144 points in the IBZ. The electronic bands are computed along the high-symmetry directions of the IBZ of pristine MgB_2C_2 shown in Fig. 3.

12 (for $A_{0.5}Mg_{0.5}B_2C_2$ only), we have fully optimized the lattice parameters of the hole-doped compounds as reported in Table I. The *a* and *b* lattice parameters (in the plane of the borocarbide hexagonal layers) do not change sizably with hole doping. Conversely, the interplanar distance (*c* axis) increases with hole concentration. This is probably due to a reduced Coulomb attraction between the negatively charged borocarbide planes and the cationic planes. For Na doping the interplanar expansion is much larger than for Li, due to the larger size of the sodium ion with respect to Mg^{2+}. The largest deformation induced by the presence of alkali metal is a displacement along the *c* direction of the carbon ions [with respect to the *z*-position average of the (BC) plane] of 0.005 or 0.012 Å for $Li_{0.125}Mg_{0.75}B_2C_2$ and $Li_{0.25}Mg_{0.75}B_2C_2$ and up to 0.152 Å for $Na_{0.25}Mg_{0.75}B_2C_2$. The resulting corrugation of the borocarbide plane is still 0.20 Å for the Li-doped compounds and 0.34 Å for the Na-doped compound. Hole doping can be realized also with Mg deficiency as shown in Fig. 2(f) which reports the band structure of the compound $Mg_{0.875}B_2C_2$, obtained from MgB_2C_2 by removing one Mg atom per unit cell from the position 8*d*. The band structure of $Mg_{0.875}B_2C_2$ is very similar to that of the isoelectronic compound $Li_{0.25}Mg_{0.75}B_2C_2$.

To assess the stability of the hole-doped compounds with respect to phase separation, we have calculated their formation energy according to the reaction

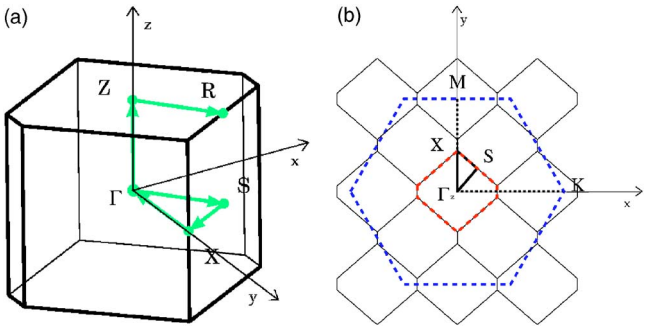

FIG. 3. (Color online) (a) Brillouin zone of MgB_2C_2. Points on the edges of the irreducible part are labeled according to Ref. 21. (b) Comparison of the projection of the Brillouin zone on the *ab* plane of MgB_2C_2 and of an ideal MgB_2 structure with B-B bond length equal to the average B-C bond length in MgB_2C_2. The BZ of ideal MgB_2 is two times larger than the BZ of MgB_2C_2 along the *c* axis and eight times larger in the *ab* plane.

$$MgB_2C_2 + xA \rightarrow A_xMg_{(1-x)}B_2C_2 + xMg \qquad (1)$$

with A=Li,Na. The pure metals are in their standard (crystalline) state.[22] Reaction (1) is endothermic for all studied concentrations of Na and Li; namely, ΔE=0.55 eV/Li for both x=0.125 and 0.25 and ΔE=0.65 eV/Li for x=0.5. The insertion energy of Li does not depend on Li content at low concentration (x=0.125–0.25). For sodium, ΔE=1.28 eV/Na at x=0.25. The larger insertion energy of Na with respect to Li is due to the larger size of the Na ion which induces a large expansion of the *c* axis (see Table I). The displacement reaction (1) is unlikely to take place for both Li and Na due to its high energy cost. However, under conditions of Mg deficiencies in the synthesis process, alkali-metal insertion might be favorable with respect to unreacted metallic alkali atoms or formation of other products. We have considered the following possible reactions in conditions of Mg deficiency:

$$Mg_{(1-x)}B_2C_2 + xLi = Li_xMg_{(1-x)}B_2C_2 \quad (\Delta E = -2.49 \text{ eV/Li}) \qquad (2)$$

$$= (MgB_2C_2)_{(1-x)} + xLiBC + \frac{x}{4}B_4C + \frac{3}{4}C \quad (-2.31) \qquad (3)$$

$$= (MgB_2C_2)_{(1-x)} + \frac{x}{2}B_4C + \frac{x}{4}LiC_6 + \frac{3}{4}xLi \quad (-1.01) \qquad (4)$$

and

$$Mg_{(1-x)}B_2C_2 + xNa = Na_xMg_{(1-x)}B_2C_2 \quad (\Delta E = -1.76 \text{ eV/Na}) \qquad (5)$$

$$= (MgB_2C_2)_{(1-x)} + xNa + \frac{x}{2}B_4C + \frac{3x}{2}C \quad (-0.23) \qquad (6)$$

$$= (MgB_2C_2)_{(1-x)} + \frac{7}{10}xNa + 2xC + \frac{x}{10}Na_3B_{20} \quad (-0.94) \qquad (7)$$

$$= (MgB_2C_2)_{(1-x)} + \frac{25}{29}xNa + \frac{2x}{29}Na_2B_{29} + 2xC \quad (-0.82). \qquad (8)$$

Reaction energies are given in parentheses in eV/atom in Eqs. (2)–(8). The reaction energy in (2) refers to x=0.125, but we recall that the formation energy per Li atom of $Li_xMg_{(1-x)}B_2C_2$ is independent of Li content for x=0.125–0.25. The total energies of the crystals in reactions (2)–(8) are either taken from experimental literature or computed from a full structural relaxation.[22] Entropic contributions and zero-point energies are neglected. Reactions (3) and (4) are all more endothermic than reaction (2) which means that under Mg deficiency, the formation of $Li_xMg_{(1-x)}B_2C_2$ solid solution is more favorable than phase separation into the products of reactions (3) and (4). The same is true for $Na_xMg_{(1-x)}B_2C_2$ [cf. reactions (5)–(8)]. Reactions (3) and (4) are not exhaustive of all possible lithium boride compounds that could be formed. Several other Li_xB_y compounds have been proposed, but only Li_2B_6 and Li_3B_{14} are well defined experimentally in terms of their composition and crystal structure.[27] Although we have not investigated the stability of the solid solution with respect to these latter compounds, the results presented here suggest that hole doping by Li insertion might be realized experimentally under conditions of Mg deficiency. A recent experimental report suggests indeed that a transition from a semiconductor to a metal could be achieved by Li doping although the exact composition of the solid solution has not been identified.[28]

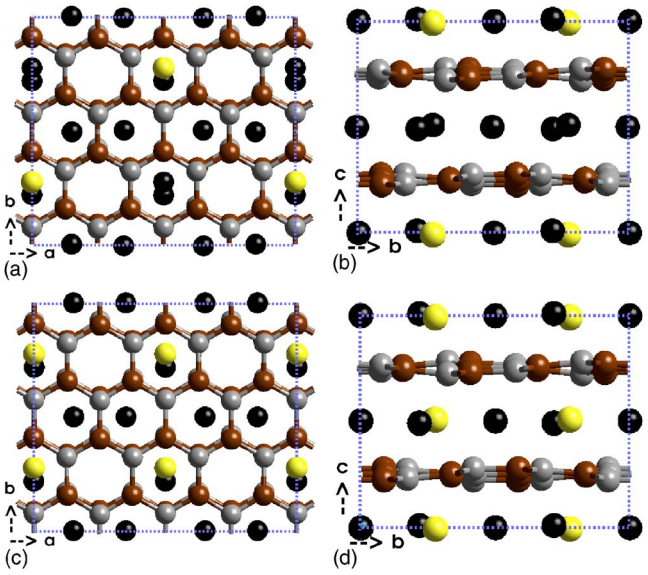

FIG. 4. (Color online) Distribution of Li ions (light gray spheres) in the elementary cell of (a) $Li_{0.125}Mg_{0.875}B_2C_2$ and (b) $Li_{0.25}Mg_{0.75}B_2C_2$. The distribution of alkali metal ions in $Na_{0.25}Mg_{0.75}B_2C_2$ is the same as in $Li_{0.25}Mg_{0.75}B_2C_2$ (cf. Fig. 1).

B. Phonons and electron-phonon interaction

Phonons of MgB_2C_2 at the Γ point can be classified according to the irreducible representations of the D_{2h} point group as $\Gamma = 15A_g + 12A_u + 15B_{1g} + 18B_{1u} + 13B_{2g} + 16B_{2u} + 17B_{3g} + 14B_{3u}$. B_{1g}, B_{2g}, B_{3g}, and A_g modes are Raman active while B_{1u}, B_{2u}, and B_{3u} modes are ir active. The ir-active modes display a dipole moment that couples to the inner macroscopic longitudinal field, which shifts the LO phonon frequencies via the non analytic contribution to the dynamical matrix[13]

$$D^{NA}_{\alpha,\beta}(\kappa,\kappa') = \frac{4\pi}{V_0}\frac{Z^*_{\alpha,\alpha'}(\kappa)q_{\alpha'}Z^*_{\beta,\beta'}(\kappa')q_{\beta'}}{\mathbf{q}\cdot\underline{\underline{\varepsilon}}^{\infty}\cdot\mathbf{q}}, \tag{9}$$

where Z^* and $\underline{\underline{\varepsilon}}^{\infty}$ are the effective charges and electronic dielectric tensors, V_0 is the unit cell volume, and $\mathbf{q}$ is the phononic wave vector. The average effective charges $Z^* = (1/3)\mathrm{Tr}\,\underline{\underline{Z^*}}$ for the eight independent atoms in the unit cell are given in Table II.

The electronic dielectric tensor is

$$\underline{\underline{\varepsilon}}^{\infty} = \begin{pmatrix} 10.2587 & & \\ & 10.2018 & \\ & & 6.0370 \end{pmatrix}. \tag{10}$$

For biaxial crystals as MgB_2C_2, the macroscopic field contribution to the dynamical matrix [Eq. (9)] introduces an angular dispersion of the phonons at the Γ point, i.e., the limit of the phononic bands $\omega(\mathbf{q})$ for $\mathbf{q}\to\mathbf{0}$ depends on the angle formed by $\mathbf{q}$ with the optical axis. The calculated phonon frequencies at the Γ point ($\mathbf{q}\to\mathbf{0}$) of the ir-active modes, for $\mathbf{q}$ parallel to the c axis, are reported in Table III for the theoretical equilibrium geometry. In this geometry only the B_{1u} modes are affected by the inner longitudinal macroscopic field (LO-TO splitting).

Although no experimental data are available on the vibrational properties of MgB_2C_2, for future reference we have computed the ir absorption spectrum for light polarized along each of the crystalline axis $(\alpha_x, \alpha_y, \alpha_z)$. The results are given in the Appendix.

It is plausible that hole-doped MgB_2C_2 might be a two-band superconductor as is the case for MgB_2 due to the similarity of the band structures of the two compounds.[4,29–33] The presence of two superconducting gaps in MgB_2 originates from the structure of the Fermi surface which is made by two separate sheets of σ and π bands.[4,32] In a multiple-band superconductor the isotropic electron-phonon coupling constant λ is decomposed into the contributions from individual bands or group of bands as

$$\lambda = \sum_{i,j}\frac{\Lambda_{ij}N_j(0)}{N(0)} = \sum_{i,j}\frac{U_{ij}N_j(0)N_i(0)}{N(0)}, \tag{11}$$

where i and j label different bands or groups of bands (e.g., $i=\sigma,\pi$), Λ_{ij} is the electron-phonon interaction matrix, and $N_i(0)$ is the contribution of the ith band to the total electronic density of states (DOS) at the Fermi level $N(0)$ (per spin and per cell).[4,29] The superconductive transition temperature T_c can be estimated from a multiband analog of the McMillan[34]

TABLE III. Theoretical phonon frequencies of MgB_2C_2 at the Γ point and oscillator strengths [f_j in Eq. (A1) in the Appendix] of ir-active u modes. The phonons are calculated in the limit $\mathbf{q}\to\mathbf{0}$ with $\mathbf{q}$ parallel to the c axis. In this geometry only the B_{1u} modes are affected by the inner longitudinal macroscopic field (LO-TO splitting). The frequencies of the B_{1u} modes without the shift due to the inner macroscopic field are reported in parentheses.

Modes	Energy (cm^{-1})	f_j
B_{1u}	164 (151)	1.665
B_{2u}	194	0.984
B_{1u}	204 (187)	0.794
B_{3u}	216	0.637
B_{3u}	236	0.535
B_{2u}	240	0.272
B_{1u}	251 (251)	0.000
B_{2u}	267	0.060
B_{2u}	329	0.257
B_{2u}	350	0.055
B_{3u}	358	0.067
B_{3u}	376	0.039
B_{1u}	395 (314)	1.705
B_{2u}	407	0.005
B_{1u}	435 (432)	0.020
B_{1u}	472 (466)	0.034
B_{3u}	510 (510)	0.000
B_{1u}	531 (529)	0.014
B_{1u}	559 (558)	0.006
B_{3u}	667	0.002
B_{2u}	678	0.001
B_{1u}	704 (704)	0.000
B_{1u}	727 (726)	0.002
B_{3u}	751	0.037
B_{1u}	754 (753)	0.007
B_{2u}	761	0.016
B_{2u}	778	0.003
B_{1u}	790 (785)	0.039
B_{3u}	806	0.002
B_{2u}	846	0.002
B_{1u}	859 (852)	0.039
B_{3u}	893	0.009
B_{2u}	1004	0.000
B_{3u}	10261	0.001
B_{2u}	1033	0.008
B_{2u}	1061	0.005
B_{3u}	1088	0.020
B_{1u}	1106 (1106)	0.000
B_{2u}	1111	0.012
B_{3u}	1112	0.001
B_{1u}	1125 (1123)	0.013
B_{1u}	1151 (1150)	0.006
B_{2u}	1195	0.816
B_{1u}	1199 (1199)	0.000
B_{3u}	1203	0.826

formula where the isotropic λ is substituted by an effective λ^{eff}, the largest eigenvalue of the matrix Λ. The matrix Λ_{ij} can be computed within DFPT as

$$\frac{\Lambda_{ij}}{N_i(0)} = \sum_{\alpha} \int \frac{d\mathbf{q}}{\Omega_{\text{BZ}}} \frac{1}{\omega^2_{\alpha\mathbf{q}}} \sum_{n\in i, m\in j} \int \frac{d\mathbf{k}}{\Omega_{\text{BZ}}} \frac{\delta(E_{\mathbf{k}n})\delta(E_{\mathbf{k}+\mathbf{q}m})}{N_i(0)N_j(0)} \times |\langle u_{\mathbf{k}+\mathbf{q},m}|\mathbf{M}^{-1/2}\boldsymbol{\epsilon}_{\alpha\mathbf{q}} \boldsymbol{\nabla} V^{\mathbf{q}}_{\text{eff}}|u_{\mathbf{k},n}\rangle|^2, \quad (12)$$

where α labels the phonons at the point $\mathbf{q}$ in the BZ (of volume Ω_{BZ}), $\boldsymbol{\epsilon}_{\alpha\mathbf{q}}$ is the phonon polarization vector, $\mathbf{M}$ is the atomic mass matrix, n and m are electronic band indices, $u_{\mathbf{k},n}$ is the periodic part of the Kohn-Sham state with energy $E_{\mathbf{k}n}$, and $\boldsymbol{\nabla} V^{\mathbf{q}}_{\text{eff}}$ is the derivative of the Kohn-Sham effective potential with respect to the atomic displacement caused by a phonon with wave vector $\mathbf{q}$. In MgB_2, Λ is a 2×2 matrix and the integral in Eq. (12) is over the σ and π sheets of the Fermi surface ($i,j=\sigma,\pi$). The element $\Lambda_{\sigma\sigma}$ is two to three times larger than the other elements (cf. Table 2 of Ref. 4). The evaluation of Eq. (12) requires a double integral over the BZ which is computationally very demanding for MgB_2C_2, containing 40 atoms per unit cell. Therefore, we restrict ourselves to the calculation of the largest element $\Lambda_{\sigma\sigma}$ to be compared with the corresponding value of MgB_2. Moreover, for systems with low dispersion of phononic and electronic bands (around the Fermi energy), a reliable estimate of the diagonal elements of Λ can be obtained in the so-called molecular like approximation as

$$\frac{\Lambda_{\sigma\sigma}}{N_\sigma(0)} = \sum_{\alpha} \frac{1}{\omega^2_{\alpha} g^2} \sum_{n,m}^{g} |\langle u_m|\mathbf{M}^{-1/2}\boldsymbol{\epsilon}_{\alpha} \boldsymbol{\nabla} V_{\text{eff}}|u_n\rangle|^2, \quad (13)$$

where the sums over α and n,m run over the phonons and the g σ bands at the Fermi level at the Γ point, respectively.[35,36] As to the applicability of Eq. (13), we have computed $\Lambda_{\sigma\sigma}$ for MgB_2 and compared our result with the values of $\Lambda_{\sigma\sigma}$ reported in Ref. 4 at full convergence in BZ integration.[37] Since the value of $\Lambda_{\sigma\sigma}$ is very sensitive to the E_{2g} phonon frequency [due to the ω^2 term in the denominator of Eq. (12)] which in turn is very sensitive to the details of the calculation (see Table 1 of Ref. 4), in order to assess the error in the approximation (13), we have renormalized our $\Lambda_{\sigma\sigma}$ with the phonon frequency obtained in the calculation at full convergence in the BZ integration we want to compare to. Referring to Table 2 of Ref. 4 the calculated values of $\Lambda_{\sigma\sigma}$ at full convergence in BZ integration fall in the range 0.78–1.02.[29,30,33] Our calculated $\Lambda_{\sigma\sigma}$ [with $N_\sigma(0)=0.15$ states/eV/spin/cell from Ref. 4] is 0.66 to be compared with the value 0.78 in Table 2 of Ref. 4. The errors in the approximation of Eq. (13) are probably even smaller for MgB_2C_2 due to the larger unit cell of MgB_2C_2 with respect to MgB_2.

For $Li_{0.125}Mg_{0.875}B_2C_2$ we obtain $\Lambda_{\sigma\sigma}/N_\sigma(0)=0.177$eV within the approximation of Eq. (13) and by including in the sum all the four highest σ bands which cross the Fermi level [see Fig. 2(b)]. All the Γ-point phonons are included. We then estimated $N_\sigma(0)$ as follows: by using the tetrahedron method (with 144 k points in the IBZ) we have computed the total DOS $N(0)$ and the DOS projected on atomic pseudo-waves-functions $\bar{N}(0)$ and $\bar{N}_\sigma(0)$ where for the latter the projection involves only the p_x, p_y, and s orbitals of B and C atoms. Due to the incompleteness of the atomic basis set $N(0)>\bar{N}(0)$. Thus $N_\sigma(0)\simeq N(0)\bar{N}_\sigma(0)/\bar{N}(0)=5.17$ states/eV/spin/cell and finally $\Lambda_{\sigma\sigma}=0.91$, which is larger than the corresponding value in MgB_2 computed within the same approximation and close to the value for MgB_2 computed at full integration in the BZ.[4] Four modes contribute for 75% to the total $\Lambda_{\sigma\sigma}$ and by adding the contribution of the other two modes we reach 90% of the total $\Lambda_{\sigma\sigma}$. All these six phonons correspond to stretching modes of the B-C bonds in the borocarbide planes and fall in the frequency range 790–885 cm^{-1}. These modes are recognizable also in the phonon spectrum of pure MgB_2C_2 although shifted at higher frequency (up to 1200 cm^{-1}). The softening of the phonons in the hole-doped compound is probably due to metallic screening. Since the effective λ^{eff} to be plugged in the multiband analog of the McMillan formula is larger than each diagonal element of Λ, a lower bound for T_c is given by

$$T_c = \frac{\omega_{\ln}}{1.2} \exp\left(-\frac{1.04(1+\Lambda_{\sigma\sigma})}{\Lambda_{\sigma\sigma}-\mu^*(1+0.62\Lambda_{\sigma\sigma})}\right), \quad (14)$$

where $\omega_{\ln}$ is the weighted logarithmic average of the phonon frequencies and μ^* is an average Coulomb pseudopotential.[34] For $Li_{0.125}Mg_{0.875}B_2C_2$ and phonons at the Γ point only, $\omega_{\ln}=777$ cm^{-1} to be compared with $\omega_{\ln}=453$ cm^{-1} for MgB_2.[29] For μ^* in the range 0.1–0.15 we finally obtain $T_c=67$–49 K.

IV. CONCLUSIONS

In summary, we have found from density functional perturbation theory that hole-doped MgB_2C_2 has a large electron-phonon coupling constant comparable to that of MgB_2. Holes can be introduced in σ bands at the Fermi level by substituting Mg with alkali metals. Calculations of the formation enthalpies show that hole-doped $Li_xMg_{(1-x)}B_2C_2$ or $Na_xMg_{(1-x)}B_2C_2$ for $x=0.125$–0.25 could be synthesized experimentally under conditions of Mg deficiencies. For $Li_{0.125}Mg_{0.875}B_2C_2$ we have found that the contribution of the σ bands to the electron-phonon coupling constant matrix (in a two-band superconductor formalism) is $\Lambda_{\sigma\sigma}=0.91$. By plugging this latter value in the McMillan formula for the critical temperature (with $\mu^*=0.1$ and the calculated $\omega_{\ln}$) we obtain $T_c=67$ K. These results show that hole-doped MgB_2C_2 might be another interesting superconductor in the class of MgB_2-like compounds.

ACKNOWLEDGMENTS

We thank M. Catti and F. Friso for discussion and information.

APPENDIX: IR SPECTRUM OF MgB_2C_2

Although no experimental data are available on the vibrational properties of MgB_2C_2, for future reference we have

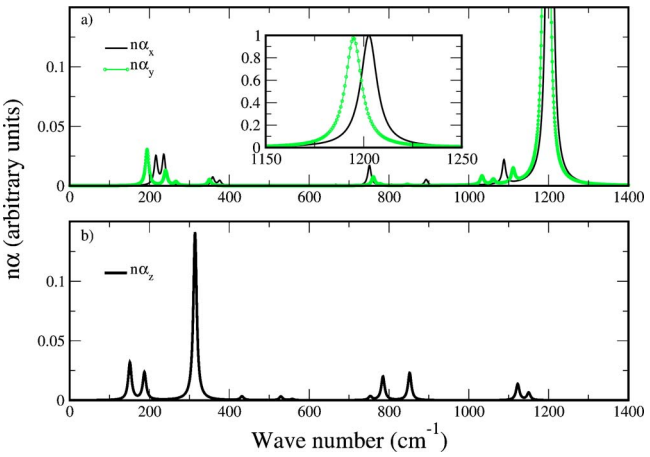

FIG. 5. (Color online) IR absorption spectrum of MgB_2C_2 for light polarized along (a) axis a ($n\alpha_x$, black line) and axis b ($n\alpha_x$, gray line) and (b) axis c ($n\alpha_x$). n is the real part of the refractive index for the given polarization.

computed the ir absorption spectrum for light polarized along each of the crystalline axes $(\alpha_x, \alpha_y, \alpha_z)$. The results are shown in Fig. 5. The absorption coefficient is obtained from phonons and effective charges as

$$\alpha(\omega) = \frac{2\pi^2}{V_o nc} \sum_{j=1}^{\nu} \left| \sum_{\kappa=1}^{N} \underline{\underline{Z}} \cdot \frac{\mathbf{e}(j,\kappa)}{\sqrt{M_\kappa}} \right|^2 \delta(\omega - \omega_j)$$

$$= \frac{\pi}{2nc} \sum_{j=1}^{\nu} f_j \omega_j^2 \delta(\omega - \omega_j), \tag{A1}$$

where c is the velocity of light in vacuum and n is the refractive index. The sum over κ run over the N atoms in the unit cell with mass M_κ. The sum over j is over phonons at the Γ point and it is restricted to B_{3u}, B_{2u}, and B_{1u} modes for α_x, α_y, and α_z, respectively. $\mathbf{e}(j,\kappa)$ and ω_j are the eigenstates and eigenvalues of the dynamical matrix at the Γ point, without the contribution of the macroscopic field, which has no effect on the phonons in the absorption geometry in which they are ir active. The coefficients f_j in Eq. (15) are reported in Table III. In the spectra shown in Fig. 5, the δ functions in Eq. (15) are approximated by Lorentzian functions as

$$\delta(\omega - \omega_j) = \frac{4}{\pi} \frac{\omega^2 \gamma}{(\omega^2 - \omega_j^2)^2 + 4\gamma^2\omega^2}, \tag{A2}$$

with $\gamma = 5\ \mathrm{cm}^{-1}$.

[1] J. Nagamatsu, N. Nakagawa, T. Muranaka, Y. Zenitani, and J. Akimitsu, Nature (London) **410**, 63 (2001).

[2] H. Rosner, A. Kitaigorodsky, and W. E. Pickett, Phys. Rev. Lett. **88**, 127001 (2002).

[3] J. M. An and W. E. Pickett, Phys. Rev. Lett. **86**, 4366 (2001).

[4] I. I. Mazin and V. P. Antropov, Physica C **385**, 49 (2003).

[5] J. K. Dewhurst, S. Sharma, C. Ambrosch-Draxl, and B. Johansson, Phys. Rev. B **68**, 020504(R) (2003).

[6] F. J. Ribeiro and M. L. Cohen, Phys. Rev. B **69**, 212507 (2004).

[7] A. Bharathi, S. J. Balaselvi, M. Premila, T. N. Sairam, G. L. N. Reddy, C. S. Sundar, and Y. Hariharan, Solid State Commun. **124**, 423 (2002).

[8] D. Souptel, Z. Hossain, G. Behr, W. Löser, and C. Geibel, Solid State Commun. **125**, 17 (2003).

[9] A. M. Fogg, P. R. Chalker, J. B. Claridge, G. R. Darling, and M. J. Rosseinsky, Phys. Rev. B **67**, 245106 (2003).

[10] A. M. Fogg, J. B. Claridge, G. R. Darling, and M. J. Rosseinsky, Chem. Commun. (Cambridge) **12**, 1348 (2003).

[11] M. Wörle and R. Nesper, J. Alloys Compd. **216**, 75 (1994).

[12] A. K. Verma, P. Modak, D. M. Gaitonde, R. S. Rao, B. K. Godwal, and L. C. Gupta, Europhys. Lett. **63**, 743 (2003).

[13] S. Baroni, S. de Gironcoli, A. Dal Corso, and P. Giannozzi, Rev. Mod. Phys. **73**, 515 (2001).

[14] A. D. Becke, Phys. Rev. A **38**, 3098 (1988); C. Lee, W. Yang, and R. G. Parr, Phys. Rev. B **37**, 785 (1988).

[15] S. Baroni *et al.*, http://www.pwscf.org

[16] N. Troullier and J. L. Martins, Phys. Rev. B **43**, 1993 (1991).

[17] S. G. Louie, S. Froyen and M. L. Cohen, Phys. Rev. B **26**, 1738 (1982).

[18] H. J. Monkhorst and J. D. Pack, Phys. Rev. B **13**, 5188 (1976).

[19] D. Murnaghan, Proc. Natl. Acad. Sci. U.S.A. **30**, 224 (1944).

[20] M. Methfessel and A. T. Paxton, Phys. Rev. B **40**, 3616 (1989).

[21] J. Zak, *Irreducible Representations of Space Groups* (Benjamin, New York, 1969).

[22] The total energy of metallic Na and Li has been computed by optimizing the lattice parameters with a $12\times12\times12$ and $10\times10\times10$ MP mesh, respectively. The resulting equilibrium lattice constant is $a=3.424$ Å for Li (expt. 3.51 Å, Ref. 23) and 4.175 Å for Na (expt. 4.29 Å, Ref. 23). The standard state of B is the rhombohedral α-B_{12} crystal. The equilibrium lattice parameter of α-B_{12}, calculated with a $5\times5\times5$ MP mesh is $a=5.135$ Å and $\alpha=59.1°$ (expt. $a=5.06$ Å and $\alpha=58.2°$, Ref. 23). The total energy of LiBC is calculated at the theoretical equilibrium lattice parameters $a=2.745$ Å and $c=3.546$ Å (expt. $a=2.752$ Å and $c=3.529$ Å, Ref. 24) with an $8\times8\times8$ MP mesh. The formation energy of C is obtained from the total energy of diamond ($a=2.878$ Å with a $10\times10\times10$ MP mesh, expt. $a=2.521$ Å, Ref. 23) and the experimental value of the energy difference between graphite and diamond. The formation energies of B_4C and LiC_6 are obtained from Refs. 25 and 26, respectively. The total energy of Na_2B_{29} is obtained by partially optimizing the $I1m1$ crystal structure (with 62 atoms per unit cell), the β angle being held fixed at the experimental value (Ref. 38). The resulting lattice parameters are $a=5.74$, $b=10.23$, $c=8.24$ Å (expt. $a=5.859$, $b=10.399$, $c=8.332$ Å and $\beta=90.373°$, Ref. 38). The total energy of Na_3B_{20} is obtained by optimizing the *Cmmm* crystal structure containing 46 atoms per unit cell with a $4\times4\times4$ MP mesh (Ref. 39). The resulting lattice parameters are $a=18.469$, $b=5.617$, $c=4.111$ Å (expt. $a=18.695$, $b=5.701$, $c=4.151$ Å, Ref. 39).

[23] N. Vast, S. Baroni, G. Zerah, J. M. Besson, A. Polian, M. Grimsditch, and J. C. Chervin, Phys. Rev. Lett. **78**, 693 (1997); N. W.

Ashcroft and N. D. Mermin, *Solid State Physics* (Holt-Saunders International Edition, Philadelphia, 1976).
[24] M. Wörle, R. Nesper, G. Mair, M. Schwarz, and H. G. von Schnering, Z. Anorg. Allg. Chem. **612**, 1153 (1995).
[25] M. W. Chase, Jr., J. Phys. Chem. Ref. Data Monogr. **9**, 1 (1998).
[26] K. R. Kganyago, P. E. Ngoepe, and C. R. A. Catlow, Solid State Ionics **159**, 21 (2003).
[27] B. Albert, Eur. J. Inorg. Chem. **8**, 1679 (2000).
[28] T. Mori, and E. Takayama-Muromachi, Curr. Appl. Phys. **4**, 276 (2004).
[29] A. Y. Liu, I. I. Mazin, and J. Kortus, Phys. Rev. Lett. **87**, 087005 (2001).
[30] H. J. Choi, D. Roundy, H. Sun, M. L. Cohen, and S. G. Louie, Phys. Rev. B **66**, 020513(R) (2002).
[31] H. J. Choi, D. Roundy, H. Sun, M. L. Cohen, and S. G. Louie, Nature (London) **418**, 758 (2002).
[32] H. J. Choi, M. L. Cohen, and S. G. Louie, Physica C **385**, 66 (2003).
[33] A. A. Gobulov, J. Kortus, O. V. Dongov, O. Jepsen, Y. Kong, O. K. Andersen, B. J. Gibson, K. Ahn, and R. K. Kremer, J. Phys.: Condens. Matter **14**, 1353 (2002).
[34] P. B. Allen and B. Mitrović, Solid State Phys. **37**, 1 (1982).
[35] M. Schluter, M. Lannoo, M. Needels, G. A. Baraff, and D. Tománek, Phys. Rev. Lett. **68**, 526 (1992).
[36] O. Gunnarsson, Rev. Mod. Phys. **69**, 575 (1997).
[37] The calculations on MgB_2 have been performed at the theoretical lattice parameters $a=3.08$ Å and $c/a=1.14$. The other computational details are the same are those reported in Sec. II. In particular, we use the gradient corrected functional of Ref. 14 while all other calculations of $\Lambda_{\sigma\sigma}$ reported in Ref. 4 are within the local density approximation.
[38] B. Albert, K. Hofmann, C. Fild, H. Eckert, M. Schleifer, and R. Gruehn, Chem.-Eur. J. **6**, 2531 (2000).
[39] B. Albert and K. Hofmann, Z. Anorg. Allg. Chem. **625**, 709 (1999).